AN EFFICIENT SCALAR AUXILIARY VARIABLE PARTITIONED PROJECTION ENSEMBLE METHOD FOR SIMULATING SURFACE-GROUNDWATER FLOWS

NAN JIANG* AND YING LI †

Abstract. We propose an efficient, partitioned, scalar auxiliary variable rotational pressure correction backward Euler (SAV-RPC-BE) ensemble scheme for simulating surface-groundwater flows modeled by the Stokes-Darcy equations. The rotational pressure correction method decouples the Stokes equations into one elliptic equation for the fluid velocity and one Poisson equation for the pressure at each time step. We incorporate the recently-developed SAV approach and the ensemble time-stepping method to further decouple the computation of the free flow region and the porous media region. The ensemble scheme results in only one common coefficient matrix shared by all realizations at each time step. Hence, efficient direct/iterative block solvers can be used to greatly reduce the computation cost. The stability analysis shows that the SAV-RPC-BE ensemble scheme is long-time stable under three parameter conditions without any time step constraints. Some numerical experiments are presented to support the theoretical results and show the effectiveness of the proposed scheme.

1. Introduction. In recent decades, the research on efficient numerical methods for the coupling of groundwater flows with surface flows (the Stokes-Darcy problem) has been developed a lot. The Stokes-Darcy model involves free flows governed by the Stokes equations and porous media flows governed by the Darcy equation. Let D_f denote the free flow region and D_p denote the porous media region, where $D_f, D_p \subset R^d$ are both open, bounded domains. The two regions lie across each other on the interface I. The Stokes-Darcy model is: to find the fluid velocity $u(x,t)$, the fluid pressure $p(x,t)$ and the hydraulic head $\phi(x,t)$ that satisfy

$$\begin{aligned} u_t - \nu\Delta u + \nabla p = f_f(x,t), \nabla\cdot u = 0, \ \text{ in } \ D_f, \\ S_0\phi_t - \nabla\cdot(\mathcal{K}(x)\nabla\phi) = f_p(x,t), \ \text{ in } \ D_p, \\ \phi(x,0) = \phi_0(x), \ \text{in } D_p \text{ and } u(x,0) = u_0(x), \ \text{in } D_f, \\ \phi(x,t) = 0, \ \text{in } \partial D_p\backslash I \text{ and } u(x,t) = 0, \ \text{in } \partial D_f\backslash I. \end{aligned} \tag{1.1}$$

The Stokes-Darcy model is coupled across the interface by three interface conditions ([1], [19], [36]). The first is the conservation of mass across I

$$u\cdot\widehat{n}_f - \mathcal{K}\nabla\phi\cdot\widehat{n}_p = 0. \tag{1.2}$$

The second interface condition is the balance of normal force across I

$$p - \nu\,\widehat{n}_f\cdot\nabla u\cdot\widehat{n}_f = g\phi. \tag{1.3}$$

The third interface condition is the Beavers-Joseph-Saffman condition on the tangential velocity

$$-\nu\widehat{\tau}_i\cdot\nabla u\cdot\widehat{n}_f = \tfrac{\alpha_{\mathrm{BJS}}}{\sqrt{\widehat{\tau}_i\cdot\mathcal{K}\widehat{\tau}_i}}u\cdot\widehat{\tau}_i. \tag{1.4}$$

Here, $\widehat{n}_{f/p}$ denotes the outward unit normal vector on I associated with $D_{f/p}$, where $\widehat{n}_f = -\widehat{n}_p$. g is the gravitational acceleration constant, $\mathcal{K}$ is the hydraulic conductivity tensor, ν is the kinematic viscosity, S_0 is the specific mass storativity coefficient. The above four coefficients are all positive. $\mathcal{K}$ is assumed to be symmetric positive definite (SPD).

Efficient numerical simulation of the time-dependent Stokes-Darcy model faces two intrinsic difficulties. The first difficulty arises from the coupling of the viscous flow governed by the Stokes equations and the porous flow governed by the Darcy equation. There have been numerous research works devoted to accurate and efficient numerical methods for decoupled schemes of the Stokes-Darcy model, e.g., [34, 37, 47, 48, 49]. However, typical time-stepping methods usually suffer from a restrictive time step condition [16, 25]. The time step condition usually comes from the decoupling of two subdomain flows and cannot be avoided without adding stabilizations [24].

The scalar auxiliary variable (SAV) approach was first studied in [52, 53] for gradient flows. The idea of it is to introduce a new scalar auxiliary variable (SAV) with an explicit treatment of the nonlinear term,

*Department of Mathematics, University of Florida, Gainesville, FL 32611, jiangn@ufl.edu. This author was partially supported by the US National Science Foundation grants DMS-2120413 and DMS-2143331.

†Department of Mathematics, University of Florida, Gainesville, FL 32611, yli7@ufl.edu. This author was partially supported by the US National Science Foundation grant DMS-2143331.

leading to an unconditional energy-stable scheme. For nonlinear Navier-Stokes equations, this idea has been realized in [28, 27, 30, 32, 41, 42, 43]. For linear Stokes-Darcy equations, the SAV approach is used to cancel out the coupling terms, which usually cause time step constraints in the stability analysis. The long-time stability without any time step conditions for first order and second order schemes was proved in [29, 31].

The second challenge is the incompressibility constraint in the Stokes equations, which couples the fluid velocity and the pressure. To decouple the fluid velocity and the pressure in incompressible flows, projection methods have been widely used, following the pioneering works of Chorin [4] and Temam [55] in the late 1960s. Projection methods have generated significant interest among researchers in recent decades, see, for instance, [6, 11, 12, 50, 51]. A comprehensive review on various projection-type methods can be found in [10]. This paper focuses specifically on pressure correction methods, which are the most commonly used projection methods. They usually involve two sub-steps per time step: (i) explicitly treating the pressure gradient in the momentum equation to solve for an intermediate velocity field and (ii) correcting the pressure by projecting the intermediate velocity onto the divergence-free space.

Pressure correction methods are typically computationally efficient, as only one elliptic equation for the velocity and one Poisson equation for the pressure are solved at each time step. However, this efficiency comes at the cost of degraded pressure approximation due to the artificial Neumann boundary condition not satisfied by the exact pressure. A modified pressure correction scheme with a divergence term added to the pressure update was introduced in [54] via a predictor-corrector procedure. This method is often referred to as the rotational pressure correction (RPC) method in the literature. Both numerical experiments and error analysis in [13] show that this method improves the pressure approximation. The rotational pressure correction method is adopted in [9] for the Stokes equations with open boundary conditions. It is presented in this paper that the RPC scheme plays an important role in approximating the Stokes equations with open boundary conditions since the standard pressure correction scheme is not well-suited for such scenarios. More recently, researchers have found that when employing pressure correction schemes, setting only Neumann boundary condition for pressure may cause some stability issues for interface problems, see [17, 18]. In [18], the authors studied and analyzed pressure correction schemes for the Fluid-Structure Interaction (FSI) problem. In this paper, they imposed the Dirichlet boundary condition for the pressure on the interface when solving the pressure Poisson equation. This is inspired by the similarity between the interface condition of the FSI model and the open boundary condition of the time-dependent Stokes equations. The idea of imposing Dirichlet boundary conditions for pressure is also adopted in [38, 39] for pressure correction methods of the coupled Stokes-Darcy model. In [9], the open boundary condition is described as

$$p\widehat{n} - \frac{1}{2}\nu\nabla u\widehat{n}|_I = 0, \tag{1.5}$$

where $\widehat{n}$ is the unit outward normal of the Stokes model. This is similar to the interface boundary condition for the balance of force (1.3) of the Stokes-Darcy model described above. If we impose Dirichlet boundary conditions on the interface, we will have two series of boundary conditions on pressure

$$\frac{\partial p^{n+1}}{\partial \widehat{n}_f}|_{\partial D_f\setminus I} = \frac{\partial p^n}{\partial \widehat{n}_f}|_{\partial D_f\setminus I} = \cdots = \frac{\partial p^1}{\partial \widehat{n}_f}|_{\partial D_f\setminus I} = \frac{\partial p^0}{\partial \widehat{n}_f}|_{\partial D_f\setminus I}, \tag{1.6}$$

$$p^{n+1}|_I = p^n|_I = \cdots = p^1|_I = p^0|_I. \tag{1.7}$$

These conditions are usually not satisfied by any exact solutions and will lead to poor pressure approximation. In this paper, we adopted the rotational pressure correction scheme to improve the bad pressure approximation due to inconsistent boundary conditions described above. The projection sub-step of the RPC scheme is described as follows.

$$\begin{cases} \dfrac{u^{n+1}-\tilde{u}^{n+1}}{\Delta t} + \nabla z^{n+1} = 0, \\ \nabla\cdot u^{n+1} = 0, \\ u^{n+1}\cdot\widehat{n}_f|_{\partial D_f\setminus I} = 0, \quad z^{n+1}|_I = 0, \\ \dfrac{\partial z^{n+1}}{\partial \widehat{n}_f}|_{\partial D_f\setminus I} = 0, \end{cases} \tag{1.8}$$

$$p^{n+1} = z^{n+1} + p^n - \chi\nu\nabla\cdot\widetilde{u}^{n+1}, \tag{1.9}$$

where $\widetilde{u}^{n+1}$ denotes the intermediate velocity and χ is a tunable positive coefficient. The pressure p^{n+1} is updated with an additional term $\chi\nu\nabla\cdot\widetilde{u}^{n+1}$ compared with the standard pressure correction method.

Our motivation for pursuing efficient simulations arises from the necessity of conducting ensemble simulations that consider uncertainties in initial conditions and forcing terms within the Navier-Stokes model. A recent ensemble algorithm was proposed in [20, 23] to address this issue, which simultaneously solves all realizations, reducing the computational cost of ensemble simulations. The algorithm is characterized by that all realizations share a common coefficient matrix for different right hand sides (RHSs), which makes it possible to use efficient block solvers such as block CG to save both the computer storage and the computational time. This ensemble time-stepping idea was further extended to simulate other PDE problems including the natural convection problem [7, 8, 21], heat equation [7, 44, 45], convection-diffusion equation [40], MHD flow [2, 3, 26, 46] and turbulent modeling [5, 22]. For the Stokes-Darcy model, uncertainties are mainly from difficulties in measuring accurate parameters, e.g., the hydraulic conductivity tensor $\mathcal{K}(x)$. The first-order ensemble schemes were studied in [16, 25]. Besides that, some higher-order ensemble schemes were also studied and proved to be highly efficient and unconditionally stable [24, 33]. In this paper, we consider the ensemble algorithm to compute an ensemble of J Stokes-Darcy systems corresponding to J different parameter sets $(\mathcal{K}_j, u_j^0, \phi_j^0, f_{f,j}, f_{p,j})$, $j = 1, ..., J$. The goal is to find J corresponding solutions (u_j, p_j, ϕ_j) to the Stokes-Darcy model:

$$\begin{aligned} u_{j,t} - \nu\Delta u_j + \nabla p_j = f_{f,j}(x,t),\ \nabla\cdot u_j = 0, \quad \text{in } D_f,\\ S_0\phi_{j,t} - \nabla\cdot(\mathcal{K}_j(x)\nabla\phi_j) = f_{p,j}(x,t), \quad \text{in } D_p,\\ \phi_j(x,0) = \phi_j^0(x), \text{ in } D_p \text{ and } u_j(x,0) = u_j^0(x), \text{ in } D_f. \end{aligned} \tag{1.10}$$

We extend the study of the first-order ensemble scheme by involving the rotational pressure correction (RPC) method and the SAV approach to further increase the efficiency of the algorithm. First, we define scalar auxiliary variables $r_j(t)$ by

$$r_j(t) = exp(-\frac{t}{T}), \quad j = 1, \ldots, J. \tag{1.11}$$

These new unknowns make it possible to cancel out the coupling terms that usually cause time step conditions in the analysis of partitioned methods. Note that real solutions $r_j(t)$ are the same for all realizations, but discrete solutions r_j^n are different. We also have

$$\frac{dr_j}{dt} = -\frac{1}{T}r_j + \frac{1}{exp(-\frac{t_{n+1}}{T})}\left(c_I(u_j,\phi_j) - c_I(u_j,\phi_j)\right), \tag{1.12}$$

where the coupling term c_I is an integral defined over the interface,

$$c_I(u,\phi) = g\int_I \phi u\cdot\widehat{n}_f\ ds.$$

The discrete form of equation (1.12) plays an important role in decoupling the free flow region and the porous media region in partitioned methods. Inspired by the idea in [9], we propose the semi-discrete scheme of our SAV rotational pressure correction (RPC) algorithm based on the backward Euler (BE) time-stepping as follows.

ALGORITHM 1.1. *(SAV-RPC-BE ensemble scheme) Step 1: Given $p_j^n, u_j^n, \widetilde{u}_j^n, \phi_j^n$, find $(\widetilde{u}_j^{n+1}, \phi_j^{n+1}) \in X_f \times X_p$ and r_j^{n+1} such that $\forall(v,\psi)\in X_f\times X_p$*

$$\begin{aligned} &\left(\frac{\widetilde{u}_j^{n+1}-u_j^n}{\Delta t}, v\right)_f + \nu(\nabla\widetilde{u}_j^{n+1}, \nabla v)_f + \sum_i\int_I \bar{\eta}_i(\widetilde{u}_j^{n+1}\cdot\widehat{\tau}_i)(v\cdot\widehat{\tau}_i)\ ds + \frac{r_j^{n+1}}{exp(-\frac{t_{n+1}}{T})}c_I(v,\phi_j^n)\\ &+\sum_i\int_I(\eta_{i,j}-\bar{\eta}_i)(\widetilde{u}_j^n\cdot\widehat{\tau}_i)(v\cdot\widehat{\tau}_i)\ ds - \left(p_j^n, \nabla\cdot v\right)_f = (f_{f,j}^{n+1}, v)_f, \end{aligned} \tag{1.13}$$

$$gS_0\left(\frac{\phi_j^{n+1}-\phi_j^n}{\Delta t},\psi\right)_p + g\left(\bar{\mathcal{K}}\nabla\phi_j^{n+1},\nabla\psi\right)_p + g\left((\mathcal{K}_j-\bar{\mathcal{K}})\nabla\phi_j^n,\nabla\psi\right)_p - \frac{r_j^{n+1}}{exp(-\frac{t_{n+1}}{T})}c_I(\widetilde{u}_j^n,\psi)$$
$$= g(f_{p,j}^{n+1},\psi)_p, \tag{1.14}$$

$$\frac{r_j^{n+1}-r_j^n}{\Delta t} = -\frac{1}{T}r_j^{n+1} + \frac{1}{exp(-\frac{t_{n+1}}{T})}\left(c_I(\widetilde{u}_j^{n+1},\phi_j^n) - c_I(\widetilde{u}_j^n,\phi_j^{n+1})\right), \tag{1.15}$$

where

$$\bar{\mathcal{K}} = \frac{1}{J}\sum_{j=1}^{J}\mathcal{K}_j, \qquad \eta_{i,j} = \frac{\alpha_{\mathrm{BJS}}}{\sqrt{\hat{\tau}_i\mathcal{K}_j\hat{\tau}_i}}, \qquad \bar{\eta_i} = \frac{1}{J}\sum_{j=1}^{J}\eta_{i,j}. \tag{1.16}$$

Step 2: Given $\widetilde{u}_j^{n+1}$, find $z_j^{n+1}\in M_f$ such that $\forall q\in M_f$

$$\begin{cases}(\nabla z_j^{n+1},\nabla q)_f = -\dfrac{1}{\Delta t}(\nabla\cdot\tilde{u}_j^{n+1},q)_f,\\ \dfrac{\partial z_j^{n+1}}{\partial\widehat{n}_f}|_{\partial D_f\backslash I} = 0.\end{cases} \tag{1.17}$$

Update $u_j^{n+1}\in X_f$ and $p_j^{n+1}\in Q_f$ by

$$u_j^{n+1} = \widetilde{u}_j^{n+1} - \Delta t\nabla z_j^{n+1}, \tag{1.18}$$
$$p_j^{n+1} = z_j^{n+1} + p_j^n - \chi\nu\nabla\cdot\widetilde{u}_j^{n+1}. \tag{1.19}$$

Definitions of corresponding spaces will be introduced in the following section.

The remainder of this paper is organized as follows. Section 2 provides some mathematical preliminaries and defines some notations. Section 3 proves the long-time stability of the SAV-RPC-BE ensemble scheme under three parameter conditions. Section 4 presents the numerical implementation of the SAV-RPC-BE ensemble algorithm. Section 5 presents numerical experiments to verify our theoritical results. Section 6 gives a conclusion.

2. Notation and preliminaries. We denote the $L^2(I)$ norm by $\|.\|_I$ and the $L^2(D_{f/p})$ norms by $\|.\|_{f/p}$; the corresponding inner products are denoted by $(.,.)_{f/p}$. Further, we denote the $H^1(D_{f/p})$ norm by $\|.\|_{1,f/p}$ and by $(.,.)_{1,f/p}$ the corresponding inner product. Let $C_{P,f}$ and $C_{P,p}$ be the Poincaré constants of the indicated domains. The following Poincaré inequalities are used in the proof.

$$\|u\|_f \le C_{P,f}\|\nabla u\|_f \qquad \text{and} \qquad \|\phi\|_p \le C_{P,p}\|\nabla\phi\|_p$$

To discretize the Stokes-Darcy problem in space by the finite element method, we choose conforming velocity, pressure, and hydraulic head spaces:

$$X_f^h \subset X_f = \{v\in\left(H^1(D_f)\right)^d : v = 0 \text{ on } \partial D_f\backslash I\},$$
$$Q_f^h \subset Q_f = H^1(D_f),$$
$$X_p^h \subset X_p = \{\psi\in H^1(D_p) : \psi = 0 \text{ on } \partial D_p\backslash I\}.$$

Here we choose $Q_f^h\subset H^1(D_f)$ as suggested in [11] since we are dealing with the projection step as a Poisson equation. We denote $M_f^h\subset M_f = \{q\in Q_f : q = 0 \text{ on } I\}$ as the finite element space of pressure increment. X_f^h and X_p^h are separate FEM spaces; continuity across the interface I is not assumed. The Stokes velocity-pressure finite element spaces, (X_f^h, Q_f^h), are assumed to satisfy the usual discrete inf-sup condition for stability of the discrete pressure, e.g., [14], [15], [35].

We propose a partitioned rotational pressure correction (RPC) ensemble scheme based on the SAV approach for the fast computation of the Stokes-Darcy model. The fully discrete algorithm with the backward Euler (BE) time-stepping is constructed as follows.

ALGORITHM 2.1. *(SAV-RPC-BE ensemble Method) Step 1: Given $p_{j,h}^n$, $u_{j,h}^n$, $\widetilde{u}_{j,h}^n$ and $\phi_{j,h}^n$, find $(\widetilde{u}_{j,h}^{n+1}, \phi_{j,h}^{n+1}) \in X_f \times X_p$ and r_j^{n+1} such that $\forall (v_h, \psi_h) \in X_f \times X_p$*

$$\left(\frac{\widetilde{u}_{j,h}^{n+1} - u_{j,h}^n}{\Delta t}, v_h\right)_f + \nu(\nabla \widetilde{u}_{j,h}^{n+1}, \nabla v_h)_f + \sum_i \int_I \bar{\eta}_i (\widetilde{u}_{j,h}^{n+1} \cdot \widehat{\tau}_i)(v_h \cdot \widehat{\tau}_i)\, ds + \frac{r_j^{n+1}}{exp(-\frac{t_{n+1}}{T})} c_I(v_h, \phi_{j,h}^n)$$
$$+ \sum_i \int_I (\eta_{i,j} - \bar{\eta}_i)(\widetilde{u}_{j,h}^n \cdot \widehat{\tau}_i)(v_h \cdot \widehat{\tau}_i)\, ds - \left(p_{j,h}^n, \nabla \cdot v_h\right)_f = (f_{f,j}^{n+1}, v_h)_f, \tag{2.1}$$

$$gS_0 \left(\frac{\phi_{j,h}^{n+1} - \phi_{j,h}^n}{\Delta t}, \psi_h\right)_p + g\left(\bar{\mathcal{K}} \nabla \phi_{j,h}^{n+1}, \nabla \psi_h\right)_p + g\left((\mathcal{K}_j - \bar{\mathcal{K}}) \nabla \phi_{j,h}^n, \nabla \psi_h\right)_p - \frac{r_j^{n+1}}{exp(-\frac{t_{n+1}}{T})} c_I(\widetilde{u}_{j,h}^n, \psi_h)$$
$$= g(f_{p,j}^{n+1}, \psi_h)_p, \tag{2.2}$$

$$\frac{r_j^{n+1} - r_j^n}{\Delta t} = -\frac{1}{T} r_j^{n+1} + \frac{1}{exp(-\frac{t_{n+1}}{T})} \left(c_I(\widetilde{u}_{j,h}^{n+1}, \phi_{j,h}^n) - c_I(\widetilde{u}_{j,h}^n, \phi_{j,h}^{n+1})\right), \tag{2.3}$$

where

$$\bar{\mathcal{K}} = \frac{1}{J} \sum_{j=1}^J \mathcal{K}_j, \qquad \eta_{i,j} = \frac{\alpha_{BJS}}{\sqrt{\hat{\tau}_i \mathcal{K}_j \hat{\tau}_i}}, \qquad \bar{\eta}_i = \frac{1}{J} \sum_{j=1}^J \eta_{i,j}. \tag{2.4}$$

Step 2: Given $\widetilde{u}_{j,h}^{n+1}$, find $z_{j,h}^{n+1} \in M_f^h$ such that $\forall q_h \in M_f^h$

$$\begin{cases} (\nabla z_{j,h}^{n+1}, \nabla q_h)_f = -\dfrac{1}{\Delta t} (\nabla \cdot \tilde{u}_{j,h}^{n+1}, q_h)_f, \\ \dfrac{\partial z_{j,h}^{n+1}}{\partial \widehat{n}_f} |_{\partial D_f \setminus I} = 0. \end{cases} \tag{2.5}$$

Update $u_{j,h}^{n+1} \in X_f^h$ and $p_{j,h}^{n+1} \in Q_f^h$ by

$$u_{j,h}^{n+1} = \widetilde{u}_{j,h}^{n+1} - \Delta t \nabla z_{j,h}^{n+1}, \tag{2.6}$$
$$p_{j,h}^{n+1} = z_{j,h}^{n+1} + p_{j,h}^n - \chi \nu \nabla \cdot \tilde{u}_{j,h}^{n+1}. \tag{2.7}$$

The method fully decouples the computation of fluid velocity, pressure and hydraulic head, which greatly improves the computing efficiency. Moreover, since it is an ensemble algorithm, at each time step, all realizations share the same coefficient matrix (for u_j, ϕ_j, p_j respectively). This further reduces the computation time.

3. Unconditional stability of SAV-RPC-BE ensemble method. Let $k_{j,min}(x), \bar{k}_{min}(x)$ be the minimum eigenvalues of $\mathcal{K}_j(x), \bar{\mathcal{K}}(x)$, respectively, and $\rho_j'(x)$ be the spectral radius of fluctuation of the hydraulic conductivity tensor $\mathcal{K}_j(x) - \bar{\mathcal{K}}(x)$, which means $|\mathcal{K}_j(x) - \bar{\mathcal{K}}(x)|_2 = \rho_j'(x)$ since $\mathcal{K}_j(x), \bar{\mathcal{K}}(x)$ are symmetric. To obtain the stability of Algorithm 2.1, we define the following notations which will be used in the proof:

$$\eta_{i,j}^{max'} = \max_{x \in I} |\eta_{i,j}(x) - \bar{\eta}_{i,j}(x)|, \qquad \eta_i^{max'} = \max_{1 \le j \le J} \eta_{i,j}^{max'}, \qquad \bar{\eta}_i^{min} = \min_{x \in I} \bar{\eta}_i(x),$$
$$\rho_j^{max'} = \max_{x \in \Omega_p} |\mathcal{K}_j(x) - \bar{\mathcal{K}}(x)|, \qquad \rho^{max'} = \max_{1 \le j \le J} \rho_j^{max'}, \qquad \bar{k}_{min} = \min_{x \in \Omega_p} \bar{k}_{min}(x).$$

Based on the idea of stability analysis in [17], we introduce a sequence $\{\xi_{j,h}^n\} \in Q_f^h$ defined by

$$\xi_{j,h}^{n+1} = \chi\nu\nabla\cdot\widetilde{u}_{j,h}^{n+1} + \xi_{j,h}^n \text{ with } \xi_{j,h}^0|_I = 0 \tag{3.1}$$

which will be used in the following stability proof.

THEOREM 3.1 (Unconditional stability of Algorithm (2.1)). *Taking $p_{j,h}^0|_I = 0$, if the following parameter conditions are satisfied,*

$$\eta_i^{max'} \le \bar{\eta}_i^{min}, \qquad \rho^{max'} < \bar{k}_{min}, \qquad \chi < \frac{2}{d}, \tag{3.2}$$

where the space dimension $d = 2, 3$, then for any $N > 0$, we have

$$\begin{aligned}
&\|u_{j,h}^N\|_f^2 + \sum_{n=0}^{N-1}\|\widetilde{u}_{j,h}^{n+1} - u_{j,h}^n\|_f^2 + (1-\frac{d\chi}{2})\Delta t\nu\sum_{n=0}^{N-1}\|\nabla\widetilde{u}_{j,h}^{n+1}\|_f^2 \\
&+ gS_0\|\phi_{j,h}^N\|_p^2 + gS_0\sum_{n=0}^{N-1}\|\phi_{j,h}^{n+1} - \phi_{j,h}^n\|_p^2 + g\Delta t\rho^{max'}\|\nabla\phi_{j,h}^N\|_p^2 + g\Delta t(\bar{k}_{min} - \rho^{max'})\sum_{n=0}^{N-1}\|\nabla\phi_{j,h}^{n+1}\|_p^2 \\
&+ \Delta t\sum_i \bar{\eta}_i^{min}\int_I \left(\widetilde{u}_{j,h}^N\cdot\widehat{\tau}_i\right)^2 ds + \Delta t^2\|\nabla(z_{j,h}^N + p_{j,h}^{N-1} + \xi_{j,h}^{N-1})\|_f^2 \\
&+ \frac{\Delta t}{\chi\nu}\|\xi_{j,h}^N\|_f^2 + |r_j^N|^2 + \sum_{n=0}^{N-1}|r_j^{n+1} - r_j^n|^2 + \frac{2\Delta t}{T}\sum_{n=0}^{N-1}|r_j^{n+1}|^2 \\
&\le \|u_{j,h}^0\|_f^2 + gS_0\|\phi_{j,h}^0\|_p^2 + \frac{\Delta t}{\chi\nu}\|\xi_{j,h}^0\|_f^2 + |r_j^0|^2 \\
&+ g\Delta t\rho^{max'}\|\nabla\phi_{j,h}^0\|_p^2 + \Delta t\sum_i \bar{\eta}_i^{min}\int_I \left(\widetilde{u}_{j,h}^0\cdot\widehat{\tau}_i\right)^2 ds + \Delta t^2\|\nabla(p_{j,h}^0 + \xi_{j,h}^0)\|_f^2 \\
&+ \Delta t\sum_{n=0}^{N-1}\frac{C_{P,f}^2}{(1-\frac{d\chi}{2})\nu}\|f_{f,j}^{n+1}\|_f^2 + \Delta t\sum_{n=0}^{N-1}\frac{gC_{P,p}^2}{(\bar{k}_{min} - \rho^{max'})}\|f_{p,j}^{n+1}\|_p^2.
\end{aligned} \tag{3.3}$$

Proof. First setting $v_h = \widetilde{u}_{j,h}^{n+1}$, $\psi_h = \phi_{j,h}^{n+1}$ for (2.1)-(2.2) in Step 1, we get

$$\begin{aligned}
&\frac{1}{2\Delta t}\|\widetilde{u}_{j,h}^{n+1}\|_f^2 - \frac{1}{2\Delta t}\|u_{j,h}^n\|_f^2 + \frac{1}{2\Delta t}\|\widetilde{u}_{j,h}^{n+1} - u_{j,h}^n\|_f^2 + \nu\|\nabla\widetilde{u}_{j,h}^{n+1}\|_f^2 \\
&+ \sum_i\int_I \bar{\eta}_i(\widetilde{u}_{j,h}^{n+1}\cdot\widehat{\tau}_i)^2 ds + \frac{r_j^{n+1}}{exp(-\frac{t_{n+1}}{T})}c_I(\widetilde{u}_{j,h}^{n+1}, \phi_{j,h}^n) - \frac{r_j^{n+1}}{exp(-\frac{t_{n+1}}{T})}c_I(\widetilde{u}_{j,h}^n, \phi_{j,h}^{n+1}) \\
&+ \frac{gS_0}{2\Delta t}\|\phi_{j,h}^{n+1}\|_p^2 - \frac{gS_0}{2\Delta t}\|\phi_{j,h}^n\|_p^2 + \frac{gS_0}{2\Delta t}\|\phi_{j,h}^{n+1} - \phi_{j,h}^n\|_p^2 \\
&+ g(\bar{\mathcal{K}}\nabla\phi_{j,h}^{n+1}, \nabla\phi_{j,h}^{n+1})_p - (p_{j,h}^n, \nabla\cdot\widetilde{u}_{j,h}^{n+1})_f \\
&= -\sum_i\int_I(\eta_{i,j} - \bar{\eta}_i)(\widetilde{u}_{j,h}^n\cdot\widehat{\tau}_i)(\widetilde{u}_{j,h}^{n+1}\cdot\widehat{\tau}_i)\, ds - g((\mathcal{K} - \bar{\mathcal{K}})\nabla\phi_{j,h}^n, \nabla\phi_{j,h}^{n+1})_p \\
&+ (f_{f,j}^{n+1}, \widetilde{u}_{j,h}^{n+1})_f + g(f_{p,j}^{n+1}, \phi_{j,h}^{n+1})_p.
\end{aligned} \tag{3.4}$$

Multiplying (2.3) by r_j^{n+1} gives

$$\frac{1}{2\Delta t}|r_j^{n+1}|^2 - \frac{1}{2\Delta t}|r_j^n|^2 + \frac{1}{2\Delta t}|r_j^{n+1} - r_j^n|^2 + \frac{1}{T}|r_j^{n+1}|^2 = \frac{r_j^{n+1}}{exp(-\frac{t_{n+1}}{T})}\left(c_I(\tilde{u}_{j,h}^{n+1}, \phi_{j,h}^n) - c_I(\widetilde{u}_{j,h}^n, \phi_{j,h}^{n+1})\right). \tag{3.5}$$

Next, plugging (2.6) into (2.5) gives

$$(\widetilde{u}_{j,h}^{n+1} - u_{j,h}^{n+1}, \nabla q_h)_f = -(\nabla \cdot \widetilde{u}_{j,h}^{n+1}, q_h)_f, \, \forall q_h \in M_f^h. \tag{3.6}$$

Integration by parts yields

$$(\nabla \cdot u_{j,h}^{n+1} - \nabla \cdot \widetilde{u}_{j,h}^{n+1}, q_h)_f + \int_{D_f} (\widetilde{u}_{j,h}^{n+1} - u_{j,h}^{n+1}) \cdot \hat{n}_f q_h ds = -(\nabla \cdot \widetilde{u}_{j,h}^{n+1}, q_h)_f, \, \forall q_h \in M_f^h. \tag{3.7}$$

Thanks to $\widetilde{u}_{j,h}^{n+1}|_{\partial D_f \setminus I} = u_{j,h}^{n+1}|_{\partial D_f \setminus I} = 0$ and $q_h|_I = 0$, the above equation reduces to

$$(\nabla \cdot u_{j,h}^{n+1} - \nabla \cdot \widetilde{u}_{j,h}^{n+1}, q_h)_f = -(\nabla \cdot \widetilde{u}_{j,h}^{n+1}, q_h)_f, \, \forall q_h \in M_f^h. \tag{3.8}$$

Thus, we have

$$(\nabla \cdot u_{j,h}^{n+1}, q_h)_f = 0, \, \forall q_h \in M_f^h. \tag{3.9}$$

Taking advantages of (3.1) and (2.7), we can rewrite (2.6) as

$$u_{j,h}^{n+1} + \Delta t \nabla (p_{j,h}^{n+1} + \xi_{j,h}^{n+1}) = \widetilde{u}_{j,h}^{n+1} + \Delta t \nabla (p_{j,h}^{n} + \xi_{j,h}^{n}). \tag{3.10}$$

Since $z_{j,h}^{n+1}|_I = 0$, we have

$$(p_{j,h}^{n+1} - p_{j,h}^{n} + \chi\nu \nabla \cdot \widetilde{u}_{j,h}^{n+1})|_I = \left((p_{j,h}^{n+1} + \xi_{j,h}^{n+1}) - (p_{j,h}^{n} + \xi_{j,h}^{n}) \right)|_I = 0. \tag{3.11}$$

By taking $p_{j,h}^0|_I = \xi_{j,h}^0|_I = 0$, the above equation can be rewritten as

$$p_{j,h}^{n+1} + \xi_{j,h}^{n+1}|_I = p_{j,h}^{n} + \xi_{j,h}^{n}|_I = \cdots = p_{j,h}^{0} + \xi_{j,h}^{0}|_I = 0. \tag{3.12}$$

Taking inner product with itself of (3.10), due to (3.12) and $\widetilde{u}_{j,h}^{n+1}|_{\partial D_f \setminus I} = u_{j,h}^{n+1}|_{\partial D_f \setminus I} = 0$ we get

$$\begin{aligned} &\|u_{j,h}^{n+1}\|_f^2 + \Delta t^2 \|\nabla (p_{j,h}^{n+1} + \xi_{j,h}^{n+1})\|_f^2 - 2\Delta t (\nabla \cdot u_{j,h}^{n+1}, (p_{j,h}^{n+1} + \xi_{j,h}^{n+1}))_f \\ &= \|\widetilde{u}_{j,h}^{n+1}\|_f^2 + \Delta t^2 \|\nabla (p_{j,h}^{n} + \xi_{j,h}^{n})\|_f^2 - 2\Delta t (\nabla \cdot \widetilde{u}_{j,h}^{n+1}, (p_{j,h}^{n} + \xi_{j,h}^{n}))_f. \end{aligned} \tag{3.13}$$

By the definition of M_f^h, $(p_{j,h}^{n+1} + \xi_{j,h}^{n+1}) \in M_f^h$. Using (3.9), the above equation reduces to

$$\|u_{j,h}^{n+1}\|_f^2 + \Delta t^2 \|\nabla (p_{j,h}^{n+1} + \xi_{j,h}^{n+1})\|_f^2 = \|\widetilde{u}_{j,h}^{n+1}\|_f^2 + \Delta t^2 \|\nabla (p_{j,h}^{n} + \xi_{j,h}^{n})\|_f^2 - 2\Delta t (\nabla \cdot \widetilde{u}_{j,h}^{n+1}, (p_{j,h}^{n} + \xi_{j,h}^{n}))_f. \tag{3.14}$$

Then by $(a-b, b) = \frac{1}{2}(a^2 - b^2 - (a-b)^2)$, the last term on the RHS of the above equation can be rewritten as

$$\begin{aligned} -2\Delta t (\nabla \cdot \widetilde{u}_{j,h}^{n+1}, (p_{j,h}^{n} + \xi_{j,h}^{n}))_f &= -2\Delta t (\nabla \cdot \widetilde{u}_{j,h}^{n+1}, p_{j,h}^{n})_f - 2\Delta t (\nabla \cdot \widetilde{u}_{j,h}^{n+1}, \xi_{j,h}^{n})_f \\ &= -2\Delta t (\nabla \cdot \widetilde{u}_{j,h}^{n+1}, p_{j,h}^{n})_f - \frac{2\Delta t}{\chi\nu} (\xi_{j,h}^{n+1} - \xi_{j,h}^{n}, \xi_{j,h}^{n})_f \\ &= -2\Delta t (\nabla \cdot \widetilde{u}_{j,h}^{n+1}, p_{j,h}^{n})_f - \frac{\Delta t}{\chi\nu} \left[\|\xi_{j,h}^{n+1}\|_f^2 - \|\xi_{j,h}^{n}\|_f^2 - \|\xi_{j,h}^{n+1} - \xi_{j,h}^{n}\|_f^2 \right]. \end{aligned} \tag{3.15}$$

Plugging (3.15) back into (3.14) and dividing it by $2\Delta t$, (3.14) can be rewritten as

$$\begin{aligned} -(\nabla \cdot \widetilde{u}_{j,h}^{n+1}, p_{j,h}^{n})_f = &\frac{1}{2\Delta t} \left(\|u_{j,h}^{n+1}\|_f^2 - \|\widetilde{u}_{j,h}^{n+1}\|_f^2 \right) + \frac{\Delta t}{2} \left(\|\nabla (p_{j,h}^{n+1} + \xi_{j,h}^{n+1})\|_f^2 - \|\nabla (p_{j,h}^{n} + \xi_{j,h}^{n})\|_f^2 \right) \\ &+ \frac{1}{2\chi\nu} \left(\|\xi_{j,h}^{n+1}\|_f^2 - \|\xi_{j,h}^{n}\|_f^2 \right) - \frac{\chi\nu}{2} \|\nabla \cdot \widetilde{u}_{j,h}^{n+1}\|_f^2. \end{aligned} \tag{3.16}$$

Here using the inequality $\|\nabla \cdot v\| \leq \sqrt{d}\|\nabla v\|$, the troublesome $\|\nabla \cdot \widetilde{u}_{j,h}^{n+1}\|_f^2$ can be bounded as

$$\|\nabla \cdot \widetilde{u}_{j,h}^{n+1}\|_f^2 \leq d\|\nabla \widetilde{u}_{j,h}^{n+1}\|_f^2. \tag{3.17}$$

Based on the above estimate, adding equations (3.4), (3.5) and (3.16) yields

$$\begin{aligned}
&\frac{1}{2\Delta t}\|u_{j,h}^{n+1}\|_f^2 - \frac{1}{2\Delta t}\|u_{j,h}^{n}\|_f^2 + \frac{1}{2\Delta t}\|\widetilde{u}_{j,h}^{n+1} - u_{j,h}^{n}\|_f^2 + (\nu - \frac{d\chi\nu}{2})\|\nabla \widetilde{u}_{j,h}^{n+1}\|_f^2 \\
&+ \sum_i \int_I \bar{\eta}_i (\widetilde{u}_{j,h}^{n+1} \cdot \widehat{\tau}_i)^2 ds + \frac{gS_0}{2\Delta t}\|\phi_{j,h}^{n+1}\|_p^2 - \frac{gS_0}{2\Delta t}\|\phi_{j,h}^{n}\|_p^2 + \frac{gS_0}{2\Delta t}\|\phi_{j,h}^{n+1} - \phi_{j,h}^{n}\|_p^2 \\
&+ g(\bar{\mathcal{K}}\nabla\phi_{j,h}^{n+1}, \nabla\phi_{j,h}^{n+1})_p + \frac{\Delta t}{2}\left(\|\nabla(p_{j,h}^{n+1} + \xi_{j,h}^{n+1})\|_f^2 - \|\nabla(p_{j,h}^{n} + \xi_{j,h}^{n})\|_f^2\right) \\
&+ \frac{1}{2\chi\nu}\left(\|\xi_{j,h}^{n+1}\|_f^2 - \|\xi_{j,h}^{n}\|_f^2\right) \\
&+ \frac{1}{2\Delta t}|r_j^{n+1}|^2 - \frac{1}{2\Delta t}|r_j^{n}|^2 + \frac{1}{2\Delta t}|r_j^{n+1} - r_j^{n}|^2 + \frac{1}{T}|r_j^{n+1}|^2 \\
&\leq -\sum_i \int_I (\eta_{i,j} - \bar{\eta}_i)(\widetilde{u}_{j,h}^{n} \cdot \widehat{\tau}_i)(\widetilde{u}_{j,h}^{n+1} \cdot \widehat{\tau}_i)\, ds - g((\mathcal{K} - \bar{\mathcal{K}})\nabla\phi_{j,h}^{n}, \nabla\phi_{j,h}^{n+1})_p \\
&+ (f_{f,j}^{n+1}, \widetilde{u}_{j,h}^{n+1})_f + g(f_{p,j}^{n+1}, \phi_{j,h}^{n+1})_p.
\end{aligned} \tag{3.18}$$

Applying Cauchy-Schwarz and Young's inequalities to the source terms, we get for any constant $\alpha_1 > 0$, $\beta_1 > 0$,

$$\begin{aligned}
&(f_{f,j}^{n+1}, \widetilde{u}_{j,h}^{n+1})_f + g(f_{p,j}^{n+1}, \phi_{j,h}^{n+1})_p \\
&\leq C_{P,f}\|f_{f,j}^{n+1}\|_f \|\nabla \widetilde{u}_{j,h}^{n+1}\|_f + gC_{P,p}\|f_{p,j}^{n+1}\|_p \|\nabla\phi_{j,h}^{n+1}\|_p \\
&\leq \frac{C_{P,f}^2}{4\alpha_1\nu}\|f_{f,j}^{n+1}\|_f^2 + \alpha_1\nu\|\nabla \widetilde{u}_{j,h}^{n+1}\|_f^2 + \frac{gC_{P,p}^2}{4\beta_1\bar{k}_{min}}\|f_{p,j}^{n+1}\|_p^2 + \beta_1 g\bar{k}_{min}\|\nabla\phi_{j,h}^{n+1}\|_p^2.
\end{aligned} \tag{3.19}$$

Two fluctuations terms are bounded as follows. Using the algebraic inequality $ab \leq \frac{1}{2}(a^2 + b^2)$,

$$\begin{aligned}
&-g\left((\mathcal{K}_j - \bar{\mathcal{K}})\nabla\phi_{j,h}^{n}, \nabla\phi_{j,h}^{n+1}\right)_p \leq g\int_{\Omega_p} |\nabla\phi_{j,h}^{n}|_2 |\mathcal{K}_j - \bar{\mathcal{K}}|_2 |\nabla\phi_{j,h}^{n+1}|_2 dx \\
&\leq g\rho^{max'}\int_{\Omega_p} |\nabla\phi_{j,h}^{n}|_2 |\nabla\phi_{j,h}^{n+1}|_2 dx \leq \frac{g\rho^{max'}}{2}\left[\|\nabla\phi_{j,h}^{n}\|_p^2 + \|\nabla\phi_{j,h}^{n+1}\|_p^2\right],
\end{aligned} \tag{3.20}$$

$$\begin{aligned}
&-\sum_i \int_I (\eta_{i,j} - \bar{\eta}_i)\left(\tilde{u}_{j,h}^{n} \cdot \widehat{\tau}_i\right)\left(\widetilde{u}_{j,h}^{n+1} \cdot \widehat{\tau}_i\right) ds \leq \sum_i \int_I |\eta_{i,j} - \bar{\eta}_i||\tilde{u}_{j,h}^{n} \cdot \widehat{\tau}_i||\widetilde{u}_{j,h}^{n+1} \cdot \widehat{\tau}_i| ds \\
&\leq \sum_i \eta_{i,j}^{max'} \int_I |\tilde{u}_{j,h}^{n} \cdot \widehat{\tau}_i||\widetilde{u}_{j,h}^{n+1} \cdot \widehat{\tau}_i| ds \leq \sum_i \frac{\eta_i^{max'}}{2}\left[\int_I (\tilde{u}_{j,h}^{n} \cdot \widehat{\tau}_i)^2 ds + \int_I (\widetilde{u}_{j,h}^{n+1} \cdot \widehat{\tau}_i)^2 ds\right].
\end{aligned} \tag{3.21}$$

Based on above estimates, (3.18) becomes

$$\begin{aligned}
&\frac{1}{2\Delta t}\left(\|u_{j,h}^{n+1}\|_f^2 - \|u_{j,h}^{n}\|_f^2\right) + \frac{1}{2\Delta t}\|\widetilde{u}_{j,h}^{n+1} - u_{j,h}^{n}\|_f^2 + (1 - \alpha_1 - \frac{d\chi}{2})\nu\|\nabla \widetilde{u}_{j,h}^{n+1}\|_f^2 \\
&+ \frac{gS_0}{2\Delta t}\left(\|\phi_{j,h}^{n+1}\|_p^2 - \|\phi_{j,h}^{n}\|_p^2\right) + \frac{gS_0}{2\Delta t}\|\phi_{j,h}^{n+1} - \phi_{j,h}^{n}\|_p^2 + (1 - \beta_1 - \frac{\rho^{max'}}{\bar{k}_{min}})g\bar{k}_{min}\|\nabla\phi_{j,h}^{n+1}\|_p^2 \\
&+ \frac{g\rho^{max'}}{2}\left[\|\nabla\phi_{j,h}^{n+1}\|_p^2 - \|\nabla\phi_{j,h}^{n}\|_p^2\right] + \sum_i [\frac{\bar{\eta}_i^{min}}{2} - \frac{\eta_i^{max'}}{2}] \int_I \left(\widetilde{u}_{j,h}^{n+1} \cdot \widehat{\tau}_i\right)^2 ds \\
&+ \sum_i \frac{\bar{\eta}_i^{min}}{2}\left[\int_I \left(\widetilde{u}_{j,h}^{n+1} \cdot \widehat{\tau}_i\right)^2 ds - \int_I \left(\widetilde{u}_{j,h}^{n} \cdot \widehat{\tau}_i\right)^2 ds\right] + \sum_i [\frac{\bar{\eta}_i^{min}}{2} - \frac{\eta_i^{max'}}{2}] \int_I \left(\widetilde{u}_{j,h}^{n} \cdot \widehat{\tau}_i\right)^2 ds
\end{aligned}$$

$$
\begin{aligned}
&+\frac{\Delta t}{2}\left(\|\nabla(p_{j,h}^{n+1}+\xi_{j,h}^{n+1})\|_f^2-\|\nabla(p_{j,h}^{n}+\xi_{j,h}^{n})\|_f^2\right)+\frac{1}{2\chi\nu}\left(\|\xi_{j,h}^{n+1}\|_f^2-\|\xi_{j,h}^{n}\|_f^2\right) \\
&+\frac{1}{2\Delta t}|r_j^{n+1}|^2-\frac{1}{2\Delta t}|r_j^{n}|^2+\frac{1}{2\Delta t}|r_j^{n+1}-r_j^{n}|^2+\frac{1}{T}|r_j^{n+1}|^2 \\
&\leq \frac{C_{P,f}^2}{4\alpha_1\nu}\|f_{f,j}^{n+1}\|_f^2+\frac{gC_{P,p}^2}{4\beta_1\bar{k}_{min}}\|f_{p,j}^{n+1}\|_p^2.
\end{aligned}
\tag{3.22}
$$

To obtain stability, the following conditions need to be satisfied.

$$
1-\alpha_1-\frac{d\chi}{2}\geq 0,\quad \frac{\bar{\eta}_i^{min}}{2}-\frac{\eta_i^{max'}}{2}\geq 0,\quad (1-\beta_1-\frac{\rho^{max'}}{\bar{k}_{min}})\geq 0. \tag{3.23}
$$

Given that χ, $\eta_i^{max'}$ and $\rho^{max'}$ are all positive, we take the following parameter constraints.

$$
0<\chi<\frac{2}{d},\quad \rho^{max'}<\bar{k}_{min},\quad \eta_i^{max'}\leq\bar{\eta}_i^{min}. \tag{3.24}
$$

Since α_1 and β_1 are arbitrary positive constants, we set

$$
\alpha_1=\frac{1}{2}(1-\frac{d\chi}{2}),\quad \beta_1=\frac{1}{2}(1-\frac{\rho^{max'}}{\bar{k}_{min}}). \tag{3.25}
$$

Then the inequality (3.22) reduces to

$$
\begin{aligned}
&\frac{1}{2\Delta t}\left(\|u_{j,h}^{n+1}\|_f^2-\|u_{j,h}^{n}\|_f^2\right)+\frac{1}{2\Delta t}\|\widetilde{u}_{j,h}^{n+1}-u_{j,h}^{n}\|_f^2+\frac{1}{2}(1-\frac{d\chi}{2})\nu\|\nabla\widetilde{u}_{j,h}^{n+1}\|_f^2 \\
&+\frac{gS_0}{2\Delta t}\left(\|\phi_{j,h}^{n+1}\|_p^2-\|\phi_{j,h}^{n}\|_p^2\right)+\frac{gS_0}{2\Delta t}\|\phi_{j,h}^{n+1}-\phi_{j,h}^{n}\|_p^2+\frac{1}{2}(1-\frac{\rho^{max'}}{\bar{k}_{min}})g\bar{k}_{min}\|\nabla\phi_{j,h}^{n+1}\|_p^2 \\
&+\frac{g\rho^{max'}}{2}\left(\|\nabla\phi_{j,h}^{n+1}\|_p^2-\|\nabla\phi_{j,h}^{n}\|_p^2\right)+\sum_i\frac{\bar{\eta}_i^{min}}{2}\left[\int_I\left(\widetilde{u}_{j,h}^{n+1}\cdot\widehat{\tau}_i\right)^2ds-\int_I\left(\widetilde{u}_{j,h}^{n}\cdot\widehat{\tau}_i\right)^2ds\right] \\
&+\frac{\Delta t}{2}\left(\|\nabla(p_{j,h}^{n+1}+\xi_{j,h}^{n+1})\|_f^2-\|\nabla(p_{j,h}^{n}+\xi_{j,h}^{n})\|_f^2\right)+\frac{1}{2\chi\nu}\left(\|\xi_{j,h}^{n+1}\|_f^2-\|\xi_{j,h}^{n}\|_f^2\right) \\
&+\frac{1}{2\Delta t}|r_j^{n+1}|^2-\frac{1}{2\Delta t}|r_j^{n}|^2+\frac{1}{2\Delta t}|r_j^{n+1}-r_j^{n}|^2+\frac{1}{T}|r_j^{n+1}|^2 \\
&\leq \frac{C_{P,f}^2}{2(1-\frac{d\chi}{2})\nu}\|f_{f,j}^{n+1}\|_f^2+\frac{gC_{P,p}^2}{2(\bar{k}_{min}-\rho^{max'})}\|f_{p,j}^{n+1}\|_p^2.
\end{aligned}
\tag{3.26}
$$

Summing up from $n=0,\ldots,N-1$, and multiplying by $2\Delta t$, we find for any $N>0$,

$$
\begin{aligned}
&\|u_{j,h}^{N}\|_f^2+\sum_{n=0}^{N-1}\|\widetilde{u}_{j,h}^{n+1}-u_{j,h}^{n}\|_f^2+(1-\frac{d\chi}{2})\Delta t\nu\sum_{n=0}^{N-1}\|\nabla\widetilde{u}_{j,h}^{n+1}\|_f^2 \\
&+gS_0\|\phi_{j,h}^{N}\|_p^2+gS_0\sum_{n=0}^{N-1}\|\phi_{j,h}^{n+1}-\phi_{j,h}^{n}\|_p^2+g\Delta t\rho^{max'}\|\nabla\phi_{j,h}^{N}\|_p^2+g\Delta t(\bar{k}_{min}-\rho^{max'})\sum_{n=0}^{N-1}\|\nabla\phi_{j,h}^{n+1}\|_p^2 \\
&+\Delta t\sum_i\bar{\eta}_i^{min}\int_I\left(\widetilde{u}_{j,h}^{N}\cdot\widehat{\tau}_i\right)^2ds+\Delta t^2\|\nabla(p_{j,h}^{N}+\xi_{j,h}^{N})\|_f^2 \\
&+\frac{\Delta t}{\chi\nu}\|\xi_{j,h}^{N}\|_f^2+|r_j^{N}|^2+\sum_{n=0}^{N-1}|r_j^{n+1}-r_j^{n}|^2+\frac{2\Delta t}{T}\sum_{n=0}^{N-1}|r_j^{n+1}|^2 \\
&\leq \|u_{j,h}^{0}\|_f^2+gS_0\|\phi_{j,h}^{0}\|_p^2+\frac{\Delta t}{\chi\nu}\|\xi_{j,h}^{0}\|_f^2+|r_j^{0}|^2 \\
&+g\Delta t\rho^{max'}\|\nabla\phi_{j,h}^{0}\|_p^2+\Delta t\sum_i\bar{\eta}_i^{min}\int_I\left(\widetilde{u}_{j,h}^{0}\cdot\widehat{\tau}_i\right)^2ds+\Delta t^2\|\nabla(p_{j,h}^{0}+\xi_{j,h}^{0})\|_f^2
\end{aligned}
\tag{3.27}
$$

$$+\Delta t\sum_{n=0}^{N-1}\frac{C_{P,f}^2}{(1-\frac{d_\chi}{2})\nu}\|f_{f,j}^{n+1}\|_f^2+\Delta t\sum_{n=0}^{N-1}\frac{gC_{P,p}^2}{(\bar{k}_{min}-\rho^{max'})}\|f_{p,j}^{n+1}\|_p^2.$$

Finally, since $\nabla(p_{j,h}^N+\xi_{j,h}^N)=\nabla z_{j,h}^N+\nabla(p_{j,h}^{N-1}+\xi_{j,h}^{N-1})$, we obtain the desired result. □

4. Numerical implementation. Let

$$S_j^{n+1}=\frac{r_j^{n+1}}{exp(-\frac{t_{n+1}}{T})},\qquad \tilde{u}_{j,h}^{n+1}=\hat{u}_{j,h}^{n+1}+S_j^{n+1}\breve{u}_{j,h}^{n+1},\qquad \phi_{j,h}^{n+1}=\hat{\phi}_{j,h}^{n+1}+S_j^{n+1}\breve{\phi}_{j,h}^{n+1}. \tag{4.1}$$

Instead of solving the original algorithm, we solve the following four subproblems for $\hat{u}_{j,h}^{n+1}$, $\hat{\phi}_{j,h}^{n+1}$, $\breve{u}_{j,h}^{n+1}$,$\breve{\phi}_{j,h}^{n+1}$ respectively.

(Sub-problem 1): Find $\hat{u}_{j,h}^{n+1}\in X_f^h$ satisfying $\forall\, v_h\in X_f^h$,

$$\begin{cases}\frac{1}{\Delta t}\left(\hat{u}_{j,h}^{n+1},v_h\right)_f+\nu(\nabla\hat{u}_{j,h}^{n+1},\nabla v_h)_f+\sum_i\int_I\bar{\eta}_i(\hat{u}_{j,h}^{n+1}\cdot\widehat{\tau}_i)(v_h\cdot\widehat{\tau}_i)\,ds\\ =(f_{f,j}^{n+1},v_h)_f+\frac{1}{\Delta t}\left(u_{j,h}^n,v_h\right)_f-\sum_i\int_I(\eta_{i,j}-\bar{\eta}_i)(\tilde{u}_{j,h}^n\cdot\widehat{\tau}_i)(v_h\cdot\widehat{\tau}_i)\,ds+\left(p_{j,h}^n,\nabla\cdot v_h\right)_f,\\ \hat{u}_{j,h}^{n+1}|_{\partial D_f\setminus I}=a_j^{n+1}.\end{cases}$$

(Sub-problem 2): Find $\hat{\phi}_{j,h}^{n+1}\in X_p^h$ satisfying $\forall\ \psi_h\in X_p^h$,

$$\begin{cases}\frac{gS_0}{\Delta t}\left(\hat{\phi}_{j,h}^{n+1},\psi_h\right)_p+g(\bar{\mathcal{K}}\nabla\hat{\phi}_{j,h}^{n+1},\nabla\psi_h)_p\\ \qquad=g(f_{p,j}^{n+1},\psi_h)_p+\frac{gS_0}{\Delta t}\left(\phi_{j,h}^n,\psi_h\right)_p-g((\mathcal{K}_j-\bar{\mathcal{K}})\nabla\phi_{j,h}^n,\nabla\psi_h)_p\\ \hat{\phi}_{j,h}^{n+1}|_{\partial D_p\setminus I}=b_j^{n+1}.\end{cases}$$

(Sub-problem 3): Find $\breve{u}_{j,h}^{n+1}\in X_f^h$ satisfying $\forall\, v_h\in X_f^h$,

$$\begin{cases}\frac{1}{\Delta t}\left(\breve{u}_{j,h}^{n+1},v_h\right)_f+\nu(\nabla\breve{u}_{j,h}^{n+1},\nabla v_h)_f+\sum_i\int_I\bar{\eta}_i(\breve{u}_{j,h}^{n+1}\cdot\widehat{\tau}_i)(v_h\cdot\widehat{\tau}_i)\,ds=-c_I(v_h,\phi_{j,h}^n),\\ \breve{u}_{j,h}^{n+1}|_{\partial D_f\setminus I}=0.\end{cases}$$

(Sub-problem 4): Find $\breve{\phi}_{j,h}^{n+1}\in X_p^h$ satisfying $\forall\ \psi_h\in X_p^h$,

$$\begin{cases}\frac{gS_0}{\Delta t}\left(\breve{\phi}_{j,h}^{n+1},\psi_h\right)_p+g(\bar{\mathcal{K}}\nabla\breve{\phi}_{j,h}^{n+1},\nabla\psi_h)_p=c_I(\tilde{u}_{j,h}^n,\psi_h),\\ \breve{\phi}_{j,h}^{n+1}|_{\partial D_f\setminus I}=0.\end{cases}$$

Now we need to derive an equation for S_j^{n+1}.

$$S_j^{n+1}=\frac{r_j^{n+1}}{exp(-\frac{t_{n+1}}{T})},\qquad\Longrightarrow\qquad r_j^{n+1}=exp(-\frac{t_{n+1}}{T})\,S_j^{n+1}. \tag{4.2}$$

Multiplying (2.3) by r_j^{n+1} gives

$$\frac{r_j^{n+1}-r_j^n}{\Delta t}\cdot r_j^{n+1}+\frac{1}{T}|r_j^{n+1}|^2-\frac{r_j^{n+1}}{exp(-\frac{t_{n+1}}{T})}\left(c_I(\tilde{u}_{j,h}^{n+1},\phi_{j,h}^n)-c_I(\tilde{u}_{j,h}^n,\phi_{j,h}^{n+1})\right)=0. \tag{4.3}$$

Plugging (4.2) into (4.3) gives

$$(\frac{1}{\Delta t}+\frac{1}{T})(r_j^{n+1})^2-\frac{1}{\Delta t}r_j^nr_j^{n+1}-S_j^{n+1}\left(c_I(\tilde{u}_{j,h}^{n+1},\phi_{j,h}^n)-c_I(\tilde{u}_{j,h}^n,\phi_{j,h}^{n+1})\right)=0,$$

$$\Longrightarrow (\frac{1}{\Delta t}+\frac{1}{T})exp(-\frac{2t_{n+1}}{T})\,(S_j^{n+1})^2-\frac{1}{\Delta t}r_j^n exp(-\frac{t_{n+1}}{T})\,S_j^{n+1}$$
$$-S_j^{n+1}\left(c_I(\hat{u}_{j,h}^{n+1}+S_j^{n+1}\breve{u}_{j,h}^{n+1},\phi_j^n)-c_I(\tilde{u}_{j,h}^n,\hat{\phi}_{j,h}^{n+1}+S_j^{n+1}\breve{\phi}_{j,h}^{n+1})\right)=0.$$

At last, we obtain the equation for S_j^{n+1} as

$$S_j^{n+1}\left(A_j^{n+1}S_j^{n+1}+B_j^{n+1}\right)=0,\qquad\Longrightarrow\qquad S_j^{n+1}=-\frac{B_j^{n+1}}{A_j^{n+1}},\tag{4.4}$$

where

$$A_j^{n+1}=(\frac{1}{\Delta t}+\frac{1}{T})exp(-\frac{2t_{n+1}}{T})-c_I(\breve{u}_{j,h}^{n+1},\phi_{j,h}^n)+c_I(\tilde{u}_{j,h}^n,\breve{\phi}_{j,h}^{n+1}),$$
$$B_j^{n+1}=-\frac{1}{\Delta t}r_j^n exp(-\frac{t_{n+1}}{T})-c_I(\hat{u}_{j,h}^{n+1},\phi_{j,h}^n)+c_I(\tilde{u}_{j,h}^n,\hat{\phi}_{j,h}^{n+1}).$$

After getting $\hat{u}_{j,h}^{n+1},\breve{u}_{j,h}^{n+1},\hat{\phi}_{j,h}^{n+1},\breve{\phi}_{j,h}^{n+1},S_j^{n+1}$ can be computed directly using formula (4.4), and then we have

$$\tilde{u}_{j,h}^{n+1}=\hat{u}_{j,h}^{n+1}+S_j^{n+1}\breve{u}_{j,h}^{n+1},\qquad\phi_{j,h}^{n+1}=\hat{\phi}_{j,h}^{n+1}+S_j^{n+1}\breve{\phi}_{j,h}^{n+1}.\tag{4.5}$$

Given $\widetilde{u}_{j,h}^{n+1}$, we can solve the pressure Poisson equation for $z_{j,h}^{n+1}\in M_f^h$,

$$\begin{cases}(\nabla z_{j,h}^{n+1},\nabla q_h)=-\dfrac{1}{\Delta t}(\nabla\cdot\tilde{u}_{j,h}^{n+1},q_h),\qquad\forall q_h\in M_f^h,\\ \dfrac{\partial z_{j,h}^{n+1}}{\partial\widehat{n}_f}|_{\partial D_f\setminus I}=0.\end{cases}\tag{4.6}$$

Then $(u_{j,h}^{n+1},p_{j,h}^{n+1})$ are updated as follows.

$$u_{j,h}^{n+1}=\widetilde{u}_{j,h}^{n+1}-\Delta t\nabla z_{j,h}^{n+1},\tag{4.7}$$
$$p_{j,h}^{n+1}=z_{j,h}^{n+1}+p_{j,h}^n-\chi\nu\nabla\cdot\widetilde{u}_{j,h}^{n+1}.\tag{4.8}$$

5. Numerical experiments.

5.1. Convergence test. We consider testing the convergence of the model on $D_f=(0,1)\times(1,2)$, $D_p=(0,1)\times(0,1)$, with interface $I=[0,1]\times\{1\}$. We set the physical parameters, g, ν, S_0, α_{BJS}, equal to one, the tunable parameter $\chi=0.25$. For the hydraulic conductivity tensor, we have

$$\mathcal{K}=\begin{bmatrix}k_{11}^j & 0\\ 0 & k_{22}^j\end{bmatrix},$$

where $j=1,\ldots,J$. For simplicity in the construction of exact solution, we assume that k_{11},k_{22} are positive independent of spatial coordinates. The exact solution, as described in [33], is constructed as following:

$$u(x,y,t)=(u_1(x,y,t),\ u_2(x,y,t)),$$
$$u_1(x,y,t)=\left(x^2(y-1)^2+\exp(y/\sqrt{k_{11}})\right)\cos(t),$$
$$u_2(x,y,t)=\left(\frac{2}{3}x(1-y)^3+k_{22}(2-\pi\sin(\pi x)\right)\cos(t),$$
$$p(x,y,t)=(2-\pi\sin(\pi x))\sin(0.5\pi y)\cos(t),$$
$$\phi(x,y,t)=(2-\pi\sin(\pi x))(1-y-\cos(\pi y))\cos(t).$$

Initial conditions, boundary conditions and forcing terms are chosen according to the exact solution. To test the convergence rate, we set time step size $T=5.0$ and $\Delta t=h$. The convergence rate is expected to be $O(\Delta t+h)=O(h)=O(\Delta t)$. This result is verified in Table 5.1.

Table 5.1: Errors and Convergence rate of SAV-RPC-BE ensemble algorithm for u, p and ϕ with $J = 3$, $\Delta t = h$ and $T = 5.0$

h	$\|u_h - u\|_{H^1}^{E,1}$	Rate	$\|u_h - u\|_{H^1}^{E,2}$	Rate	$\|u_h - u\|_{H^1}^{E,3}$	Rate
1/8	2.08×10^{-1}	-	2.09×10^{-1}	-	2.11×10^{-1}	-
1/16	1.02×10^{-1}	1.02	1.03×10^{-2}	1.03	1.03×10^{-1}	1.03
1/32	4.98×10^{-2}	1.04	4.99×10^{-2}	1.04	5.00×10^{-2}	1.05
1/64	2.47×10^{-2}	1.01	2.47×10^{-2}	1.01	2.47×10^{-2}	1.02
h	$\|p_h - p\|_{L^2}^{E,1}$	Rate	$\|p_h - p\|_{L^2}^{E,2}$	Rate	$\|p_h - p\|_{L^2}^{E,3}$	Rate
1/8	1.29×10^{-1}	-	1.28×10^{-1}	-	1.28×10^{-1}	-
1/16	5.88×10^{-2}	1.13	5.71×10^{-2}	1.17	5.61×10^{-2}	1.19
1/32	3.03×10^{-2}	0.96	2.90×10^{-2}	0.98	2.81×10^{-2}	1.00
1/64	1.60×10^{-2}	0.92	1.54×10^{-2}	0.91	1.50×10^{-2}	0.90
h	$\|\phi_h - \phi\|_{H^1}^{E,1}$	Rate	$\|\phi_h - \phi\|_{H^1}^{E,2}$	Rate	$\|\phi_h - \phi\|_{H^1}^{E,3}$	Rate
1/8	6.90×10^{-2}	-	3.79×10^{-2}	-	4.43×10^{-2}	-
1/16	3.57×10^{-2}	0.95	1.97×10^{-2}	0.94	2.20×10^{-2}	1.00
1/32	1.81×10^{-2}	0.98	1.00×10^{-2}	0.98	1.10×10^{-2}	1.00
1/64	9.01×10^{-3}	1.00	4.95×10^{-3}	1.00	5.49×10^{-3}	1.00

Table 5.2: CPU time and mean error of ϕ at final time $T = 1$ with $h = 1/64, \Delta t = 1/64$

	SAV-RPC-BE ensemble		**SAV-RPC-BE non-ensemble**	
J	$\|\mathbb{E}[\phi_h - \phi]\|_{H^1}$	**CPU time**	$\|\mathbb{E}[\phi_h - \phi]\|_{H^1}$	**CPU time**
1	5.70×10^{-3}	34.5 s	5.70×10^{-3}	40.1 s
10	5.45×10^{-3}	151.4 s	5.82×10^{-3}	389.8 s
100	5.00×10^{-3}	692.4 s	5.68×10^{-3}	4232.7 s

5.2. Efficiency test. We then test the efficiency of the SAV-RPC-BE ensemble method and compare it with the corresponding non-ensemble method. For efficiency tests in this section, we still use the exact solutions and parameters stated in the previous section. The varying hydraulic conductivity tensor values k_{11}^j and k_{22}^j are uniformly distributed in the interval $[1, 2]$. We set $h = 1/64$, $\Delta t = 1/64$ and the final time $T = 1.0$. CG solver is used to solve the non-ensemble algorithm since the coefficient matrix is symmetric positive definite while block CG solver is used to solve the ensemble algorithm. We list the results of SAV-RPC-BE ensemble method and the results of SAV-RPC-BE non-ensemble method under same conditions except for varying numbers of samples: $J = 1, 10, 100$. As illustrated in Table 5.2 and 5.3, both algorithms reach the same level of accuracy for u and ϕ respectively while huge differences exist in the computation time. The CPU time of the SAV-RPC-BE ensemble method is around 86.0%, 38.8% and 16.4% of the CPU time of the SAV-RPC-BE non-ensemble method when J is 1, 10 and 100 respectively. The advantage of the ensemble scheme is obvious compared with the non-ensemble one when J is large. This is because the ensemble scheme shares a common coefficient matrix for all the realizations and the associated system with different right hand sizes (RHSs) can be solved simultaneously by the block CG solver.

5.3. Stochastic example. Next, we consider the stochastic Stokes-Darcy model with random hydraulic conductivity tensor $\mathcal{K}(x, y, \omega)$, which is a correlation function constructed as follows

$$\mathcal{K}(x, y, \omega) = \begin{bmatrix} k_{11}(x, y, \omega) & 0 \\ 0 & k_{22}(x, y, \omega) \end{bmatrix},$$

Table 5.3: Mean error of u and p at final time $T = 1$ with $h = 1/64, \Delta t = 1/64$.

	SAV-RPC-BE ensemble		**SAV-RPC-BE non-ensemble**	
J	$\|\mathbb{E}[u_h - u]\|_{H^1}$	$\|\mathbb{E}[p_h - p]\|_{L_2}$	$\|\mathbb{E}[u_h - u]\|_{H^1}$	$\|\mathbb{E}[p_h - p]\|_{L_2}$
1	2.21×10^{-2}	1.39×10^{-2}	2.22×10^{-2}	1.39×10^{-2}
10	2.21×10^{-2}	1.40×10^{-2}	2.21×10^{-2}	1.40×10^{-2}
100	2.21×10^{-2}	1.39×10^{-2}	2.21×10^{-2}	1.39×10^{-2}

Table 5.4: CPU time for sparse-grid method with $J = 241$ collocation points, $T = 1.0,\ h = 1/64,\ \Delta t = 1/100$.

	SAV-RPC-BE ensemble	**SAV-RPC-BE non-ensemble**
CPU time	3125.5 s	12906.0 s
Percentage	24.2%	100%

$$k_{11}(x,y,\omega) = k_{22}(x,y,\omega) = a_0 + \sigma\sqrt{\lambda_0}Y_0(\omega) + \sum_{i=1}^{n_f} \sigma\sqrt{\lambda_i}[Y_i(\omega)\cos(i\pi x) + Y_{n_f+i}(\omega)\sin(i\pi x))],$$

where $\lambda_0 = \frac{\sqrt{\pi}L_c}{2}$, $\lambda_i = \sqrt{\pi}L_c e^{-\frac{(i\pi L_c)^2}{4}}$ for $i = 1, \cdots, n_f$. $Y_0, \cdots, Y_{2n_f}$ are independent and identically uniformly distributed in the interval $[-\sqrt{3}, \sqrt{3}]$, so they have zero mean and unit variance. In the above KL expansion of random variables $k_{11}(x,y,\omega), k_{22}(x,y,\omega)$, we take $n_f = 2$, so there are totally 5 uncorrelated variables $Y_0, Y_1, \cdots, Y_4$. The other values are taken as $L_c = 0.25, \quad a_0 = 1, \quad \sigma = 0.15$. We set Dirichlet boundary condition and initial condition by

$$\begin{aligned}
&u(x,y,t,\omega) = (u_1(x,y,t,\omega),\ u_2(x,y,t,\omega)),\\
&u_1(x,y,t,\omega) = Y_0(\omega)(y^2 - 2y + 1)cos(t),\\
&u_2(x,y,t,\omega) = Y_1(\omega)(x^2 - x)cos(t),\\
&\phi(x,y,t,\omega) = Y_2(\omega)ycos(t).
\end{aligned}$$

The problem is associated with the forcing terms

$$f_f = (Y_3(\omega)xy, Y_3(\omega)xy), \quad f_p = Y_4(\omega)xy.$$

The SAV-RPC-BE ensemble method in this test is incorporated with the multi-grid method to approximate the stochastic Stokes-Darcy model. Sample points are selected by the sparse grid collocation method utilizing the Smolyak formula and Gaussian quadrature rule. The construction of sparse grids follows open source sparse grid codes found in:`http://www.sparse-grids.de`. We set $h = 1/64$ and $dt = 1/100$, $J = 241$ collocation points at accuracy level 4. The simulation at time $T = 1.0$ is shown in Figure 5.1. It shows that the ensemble scheme and the non-ensemble scheme obtain almost the same simulation results. The results of the computation time of corresponding simulations are listed in Table 5.4

5.4. Realistic example. Next, we apply the proposed method to a more realistic simulation of subsurface flows in a karst aquifer, inspired by test 5.3 in [16]. As shown in Figure 5.2, the free flow region D_f is a Y-shape conduit that has a curvy interface with the porous media region D_p. The closed curvy boundary of D_f is $\overline{ABCDEFGH}$ with $A = (0, 0.8)$, $B = (0, 0.55)$, $C = (0.5, 0.4)$, $D = (0.6, 0)$, $E = (0.85, 0)$, $F = (0.75, 0.45)$, $G = (1, 0.5)$, and $H = (1, 0.7)$.

Let interface $I = \bar{D}_p \cap \bar{D}_f$. Physical parameters are chosen the same as the convergence test. Set source terms to be zero and $\phi = 0$ on $\partial D_p \backslash I$. Inflow/outflow boundary conditions of u are

$$\mathbf{u} = \begin{cases} u_1 = s_1, \quad u_2 = 0, \quad on \quad \overline{AB} \\ u_1 = 0, \quad u_2 = s_2, \quad on \quad \overline{DE} \\ u_1 = s_3, \quad u_2 = 0, \quad on \quad \overline{GH} \end{cases}$$

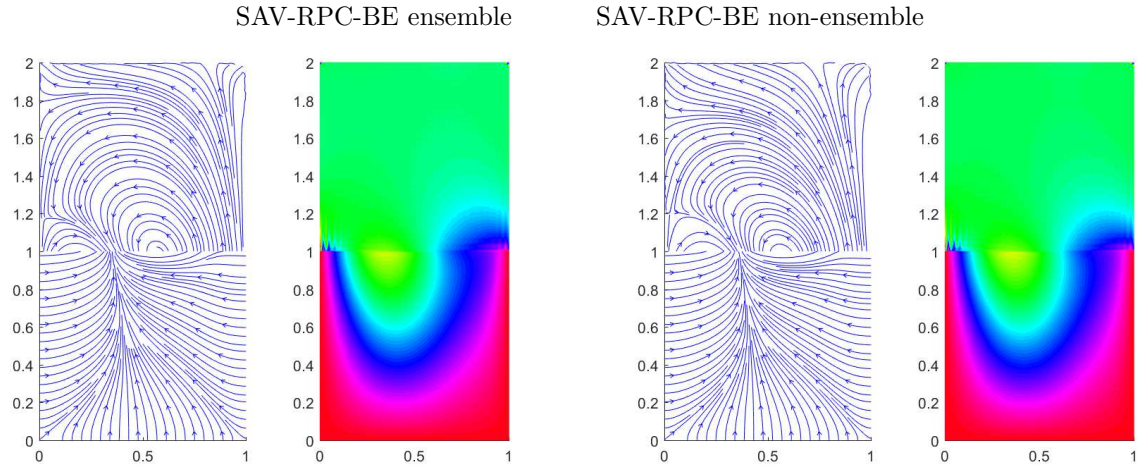

Fig. 5.1: Simulation at $T = 1.0$, with $h = 1/64, \Delta t = 1/100$ by SAV-RPC-BE ensemble (left), SAV-RPC-BE non-ensemble (right) with $J = 241$ collocation points. Count from left to right: figures 1 and 3 are streamlines of expectations of flow velocity u and $v = -\mathcal{K}\nabla\phi$, figures 2 and 4 are expectations of pressure p and hydraulic head ϕ.

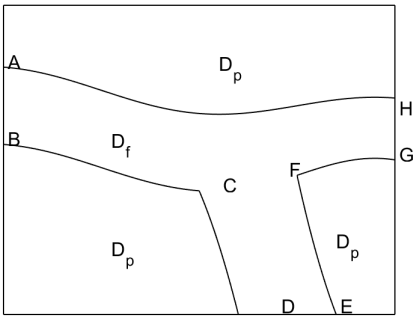

Fig. 5.2: curvy domain for simulating the karst aquifer

where s_1, s_2 and s_3 are constants. In numerical experiments, we take time step $t = 0.005$, space steps $h = 0.022$, and the simulation solutions are computed at $T = 1.0$.

Set boundary conditions $s_1 > 0$, $s_2 < 0$, and $s_3 > 0$ so that the subsurface fluid flows in through $\overline{AB}$ and out through $\overline{DE}$ and $\overline{GH}$. Figure 5.3 and 5.4 plot expectations of fluid flow velocity $\mathbb{E}[u]$, porous media flow velocity $\mathbb{E}[v]$, pressure $\mathbb{E}[p]$ and hydraulic head $\mathbb{E}[\phi]$ computed under different boundary conditions or magnitude of hydraulic conductivity. In Figure 5.3, We keep the same outflow velocity $s_2 = -1$, $s_3 = 1$ while varying the inflow velocity $s_1 = 1$, 2 and 3. One can see that compared with the balanced inflow/outflow rate in Figure 5.3 (middle), less inflow rate in Figure 5.3 (left) causes more water to be pushed into the conduit from the porous media region, which happens during a dry season; more inflow rate in Figure 5.3 (right) causes more water to be pushed into the porous media from the conduit, which happens during a rainy season.

We also consider setting small values for hydraulic conductivity $\mathcal{K}$ and specific mass storativity coefficient S_0, which is more meaningful to better align with realistic cases. We set $S_0 = 10^{-5}$ and $\alpha_{\text{BJS}} = 0.1$. We compare the effect of different $\mathcal{K}$. See $\mathcal{K} = 10^0 * I$ in Figure 5.4 (top), $\mathcal{K} = 10^{-2} * I$ in Figure 5.4 (middle) and $\mathcal{K} = 10^{-4} * I$ in Figure 5.4 (bottom). The simulations basically follow the same pattern but slower flow speeds in the Darcy domain are observed as expected when hydraulic conductivity decreases.

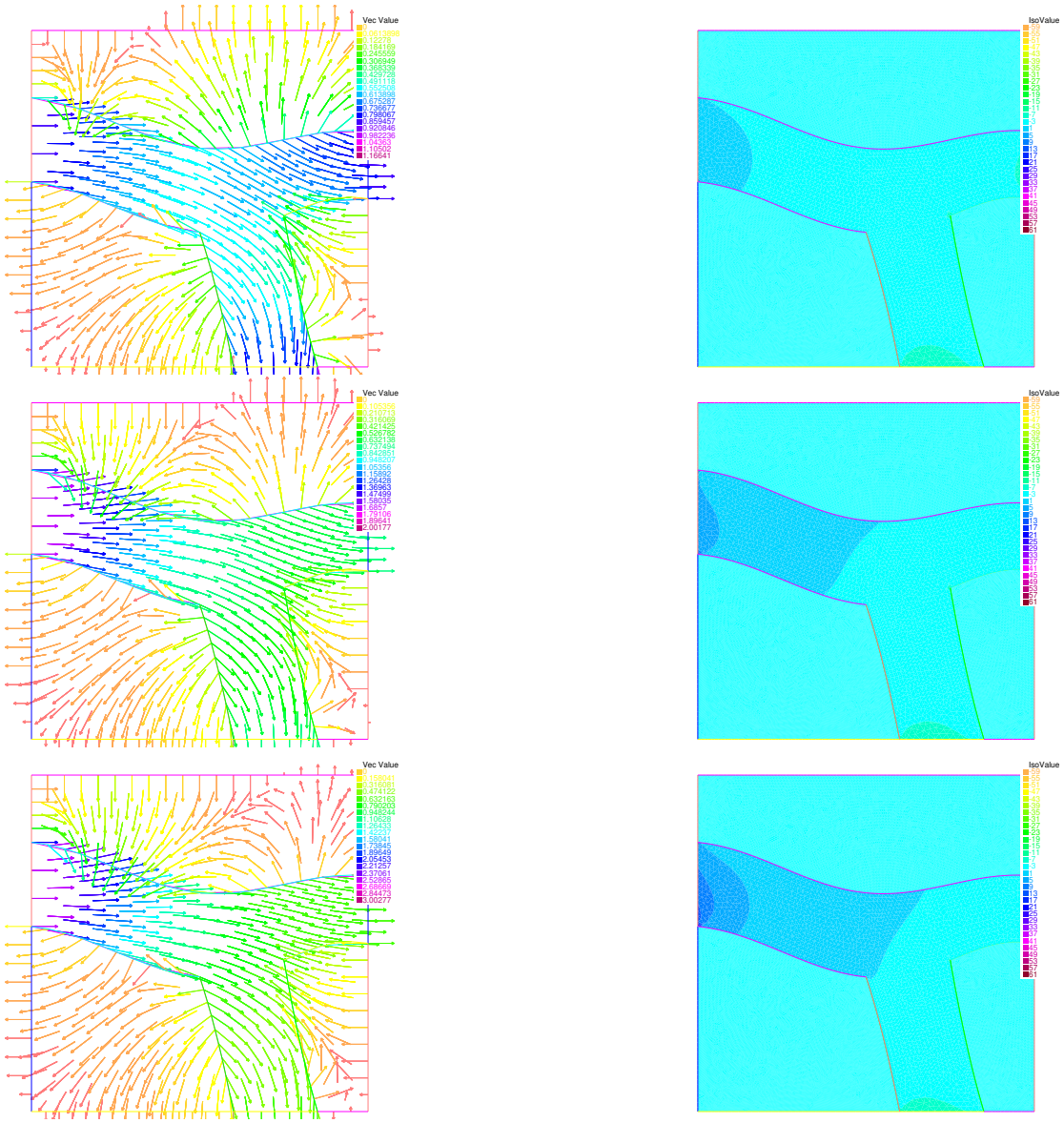

Fig. 5.3: Left: expectations of the fluid flow velocity $\mathbb{E}[u]$ and porous media flow velocity $\mathbb{E}[v]$. Right: expectations of pressure $\mathbb{E}[p]$ and hydraulic head $\mathbb{E}[\phi]$. SAV-RPC-BE ensemble algorithm with inflow velocity $s_1 = 1$ (top line), $s_1 = 2$ (middle line), $s_3 = 3$ (bottom line), fixed $s_2 = -1$, $s_3 = 1$, and fixed hydraulic conductivity $\mathcal{K} = 1.0 * \mathcal{I}$.

6. Conclusion. We constructed a first-order rotational pressure correction ensemble scheme using the idea of SAV for efficiently computing the Stokes-Darcy model. The SAV-RPC-BE ensemble scheme is extremely efficient due to two reasons: i) the fully decoupled computation of velocity, pressure, and hydraulic head resulting in smaller linear systems; ii) all ensemble members share the same coefficient matrix. The algorithm is proved to be long-time stable under three parameter conditions without any time step conditions. The numerical experiments show that the algorithm is first order as expected. The superiority of the ensemble algorithm over the non-ensemble algorithm is also demonstrated in numerical tests. Realistic examples on a curvy geometric domain simulating the karst aquifer is also presented.

REFERENCES

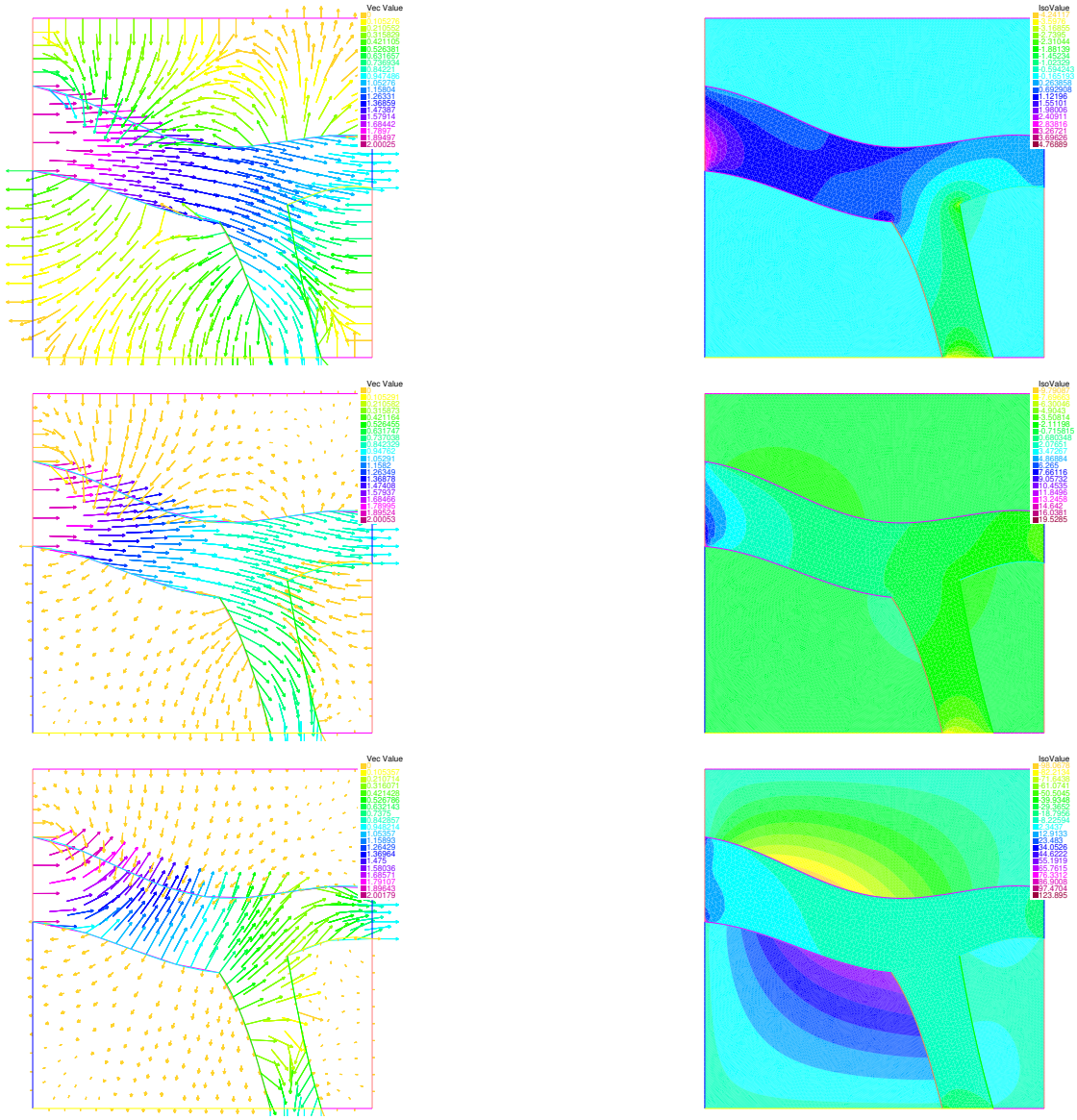

Fig. 5.4: Left: expectations of fluid flow velocity $\mathbb{E}[u]$ and porous media flow velocity $\mathbb{E}[v]$. Right: expectations of pressure $\mathbb{E}[p]$ and hydraulic head $\mathbb{E}[\phi]$. SAV-RPC-BE ensemble algorithm with hydraulic conductivity $\mathcal{K} = 10^0 * \mathcal{I}$ (top), $\mathcal{K} = 10^{-2} * \mathcal{I}$ (middle), $\mathcal{K} = 10^{-4} * \mathcal{I}$ (bottom), $S_0 = 10^{-5}$ and fixed boundary conditions $s_1 = 2$, $s_2 = -1$, $s_3 = 1$.

[1] G. Beavers and D. Joseph, *Boundary conditions at a naturally impermeable wall*, Journal of Fluid Mechanics, 30 (1) (1967), pp.197-207.

[2] J. Carter and N. Jiang, *Numerical analysis of a second order ensemble method for evolutionary Magnetohydrodynamics equations at small magnetic Reynolds number*, Numerical Methods for Partial Differential Equations, 38 (2022), 1407-1436.

[3] J. Carter, D. Han and N. Jiang, *Second order, unconditionally stable, linear ensemble algorithms for the Magnetohydrodynamics equations*, Journal of Scientific Computing, 94 (2023), 41.

[4] A.J. Chorin, *Numerical solution of the Navier-Stokes equations*, Mathematics of Computation, 22 (104) (1968), pp.745-762.

[5] J. Connors, *An ensemble-based conventional turbulence model for fluid-fluid interactions*, International Journal of Numerical Analysis and Modeling, 15 (2018), pp.492-519.

[6] E. Weinan and J. Liu, *Projection method I: convergence and numerical boundary layers*, SIAM Journal on Numerical

Analysis, 32 (1995), pp.1017-1057.
[7] J. Fiordilino, *A second order ensemble timestepping algorithm for natural convection*, SIAM Journal on Numerical Analysis, 56 (2) (2018), pp.816-837.
[8] J. Fiordilino and S. Khankan, *Ensemble timestepping algorithms for natural convection*, International Journal of Numerical Analysis and Modeling, 15 (4-5) (2018), pp.524-551.
[9] J.L. Guermond, P. Minev and J. Shen, *Error analysis of pressure-correction schemes for the time-dependent Stokes equations with open boundary conditions*, SIAM Journal on Numerical Analysis, 43 (1) (2005), pp.239-258.
[10] J.L. Guermond, P. Minev and J. Shen, *An overview of projection methods for incompressible flows*, Computer Methods in Applied Mechanics and Engineering, 195 (44-47) (2006), pp.6011–6045.
[11] J.L. Guermond and L. Quartapelle, *On the approximation of the unsteady Navier–Stokes equations by finite element projection methods*, Numerische Mathematik, 80 (1998), pp.207-238.
[12] J.L. Guermond and J. Shen, *Velocity-correction projection methods for incompressible flows*, SIAM Journal on Numerical Analysis, 41 (1) (2003), pp.112–134.
[13] J.L. Guermond and J. Shen, *On the error estimates for the rotational pressure-correction projection methods*, Mathematics of Computation, 73 (248) (2004), pp.1719–1737.
[14] M.D. Gunzburger, *Finite Element Methods for Viscous Incompressible Flows - A Guide to Theory, Practices, and Algorithms*, Academic Press, (1989).
[15] V. Girault and P. Raviart, *Finite Element Approximation of the Navier-Stokes Equations*, Lecture Notes in Mathematics, 749 (1979).
[16] X. He, N. Jiang and C. Qiu, *An artificial compressibility ensemble algorithm for a stochastic Stokes-Darcy model with random hydraulic conductivity and interface conditions*, International Journal for Numerical Methods in Engineering, 121 (4) (2020), pp.712-739.
[17] Y. He and J. Shen, *Unconditionally stable pressure-correction schemes for a nonlinear fluid-structure interaction model*, Communications on Applied Mathematics and Computation, 1 (1) (2019), pp.61-80.
[18] Y. He and J. Shen, *Unconditionally stable pressure-correction schemes for a linear fluid-structure interaction problem*, Numerical Mathematics: Theory, Methods and Applications, 7 (4) (2014), pp.537-554.
[19] W. Jäger and A. Mikelic, *On the interface boundary condition of Beavers, Joseph, and Saffman*, SIAM Journal on Applied Mathematics, 60 (4) (2000), pp.1111-1127.
[20] N. Jiang, *A higher order ensemble simulation algorithm for fluid flows*, Journal of Scientific Computing, 64 (1) (2015), pp.264-288.
[21] N. Jiang, *A pressure-correction ensemble scheme for computing evolutionary Boussinesq equations*, Journal of Scientific Computing, 80 (2019), pp.315-350.
[22] N. Jiang, S. Kaya, and W. Layton, *Analysis of model variance for ensemble based turbulence modeling*, Computational Methods in Applied Mathematics, 15 (2) (2015), pp.173-188.
[23] N. Jiang and W. Layton, *An algorithm for fast calculation of flow ensembles*, International Journal for Uncertainty Quantification, 4 (4) (2014), pp.273-301.
[24] N. Jiang, Y. Li and H. Yang, *An artificial compressibility CNLF method for the Stokes-Darcy model and application in ensemble simulations*, SIAM Journal on Numerical Analysis, 59 (1) (2021), pp.401-428.
[25] N. Jiang and C. Qiu, *An efficient ensemble algorithm for numerical approximation of stochastic Stokes-Darcy equations*, Computer Methods in Applied Mechanics and Engineering, 343 (2019), pp.249-275.
[26] N. Jiang, and M. Schneier, *An efficient, partitioned ensemble algorithm for simulating ensembles of evolutionary MHD flows at low magnetic Reynolds number*, Numerical Methods for Partial Differential Equations, 34 (6) (2018), pp.2129-2152.
[27] N. Jiang, A. Takhirov and J. Waters, *Robust SAV-ensemble algorithms for parametrized flow problems with energy stable open boundary conditions*, Computer Methods in Applied Mechanics and Engineering, 392 (2022), 114709.
[28] N. Jiang and H. Yang, *Stabilized SAV ensemble algorithms for parameterized flow problems*, SIAM Journal on Scientific Computing, 43 (4) (2021), pp.A2869-A2896.
[29] N. Jiang and H. Yang, *SAV decoupled ensemble algorithms for fast computation of Stokes-Darcy flow ensembles*, Computer Methods in Applied Mechanics and Engineering, 387 (2021), 114150.
[30] N. Jiang and H. Yang, *Numerical investigation of two second-order, stabilized SAV ensemble methods for the Navier-Stokes equations*, Advances in Computational Mathematics, 48 (2022), 65.
[31] N. Jiang and H. Yang, *Fast and accurate artificial compressibility ensemble algorithms for computing parameterized Stokes-Darcy flow ensembles*, Journal of Scientific Computing, 94 (2023), 17.
[32] N. Jiang and H. Yang, *Artificial compressibility SAV ensemble algorithms for the incompressible Navier-Stokes equations*, Numerical Algorithms, 92 (2023), 2161-2188.
[33] N. Jiang, Y. Li and H. Yang, *A second order ensemble method with different subdomain timesteps for simulating coupled surface-groundwater flows*, Numerical Methods for Partial Differential Equations, 38 (6) (2022), pp.1880-1907.
[34] M. Kubacki and M. Moraiti, *Analysis of a second-order, unconditionally stable, partitioned method for the evolutionary Stokes-Darcy model*, International Journal of Numerical Analysis and Modeling, 12 (4) (2015), pp.704-730.
[35] W. Layton, *Introduction to the Numerical Analysis of Incompressible Viscous Flows*, Society for Industrial and Applied Mathematics (SIAM), Philadelphia, (2008).
[36] W. Layton, F. Schieweck and I. Yotov,*Coupling fluid flow with porous media flow*, SIAM Journal on Numerical Analysis, 40 (6) (2002), pp.2195-2218.
[37] W. Layton, H. Tran and C. Trenchea, *Analysis of long time stability and errors of two partitioned methods for uncoupling evolutionary groundwater-surface water flows*, SIAM Journal on Numerical Analysis, 51 (51) (2013), pp.248-272.
[38] J. Li, M. Yao, M.A. Al Mahbub, and H. Zheng, *The efficient rotational pressure-correction schemes for the coupling Stokes/Darcy problem*, Computers & Mathematics with Applications, 79 (2) (2020), pp.337-353.

[39] W. Li, J. Fang, Y. Qin and P. Huang, *Rotational pressure-correction method for the Stokes/Darcy model based on the modular grad-div stabilization*, Applied Numerical Mathematics, 160 (2021), pp.451-465.
[40] N. Li, J. Fiordilino and X. Feng, *Ensemble time-stepping algorithm for the convection-diffusion equation with random diffusivity*, Journal of Scientific Computing, 79 (2019), pp.1271-1293.
[41] X. Li and J. Shen, *Error analysis of the SAV-MAC scheme for the Navier-Stokes equations*, SIAM Journal on Numerical Analysis, 58 (5) (2020), pp.2465-2491.
[42] X. Li, J. Shen and Z. Liu, *New SAV-pressure correction methods for the Navier-Stokes equations: stability and error analysis*, Mathematics of Computation, 91 (333) (2022), pp.141-167.
[43] L. Lin, Z. Yang and S. Dong, *Numerical approximation of incompressible Naiver-Stokes equations based on an auxiliary energy variable*, Journal of Computational Physics, 388 (2019), pp.1-22.
[44] Y. Luo and Z. Wang, *An ensemble algorithm for numerical solutions to deterministic and random parabolic PDEs*, SIAM Journal on Numerical Analysis, 56 (2) (2018), pp.859-876.
[45] Y. Luo and Z. Wang, *A multilevel Monte Carlo ensemble scheme for random parabolic PDEs*, SIAM Journal on Scientific Computing, 41 (1) (2019), pp.A622-A642.
[46] M. Mohebujjaman and L. Rebholz, *An efficient algorithm for computation of MHD flow ensembles*, Computational Methods in Applied Mathematics, 17 (2017), 121-137.
[47] M. Mu and X. Zhu, *Decoupled schemes for a non-stationary mixed Stokes-Darcy model*, Mathematics of Computation, 79 (270) (2010), pp.707-731.
[48] L. Shan, H. Zheng, and W. Layton, *A decoupling method with different subdomain time steps for the nonstationary Stokes–Darcy model*, Numerical Methods for Partial Differential Equations, 29 (2) (2013), pp.549-583.
[49] L. Shan and H. Zheng, *Partitioned time stepping method for fully evolutionary Stokes–Darcy flow with Beavers–Joseph interface conditions*, SIAM Journal on Numerical Analysis, 51 (2) (2013), pp.813–839.
[50] J. Shen, *On error estimates of projection methods for Navier–Stokes equations: first-order schemes*, SIAM Journal on Numerical Analysis, 29 (1) (1992), pp.57–77.
[51] J. Shen, *On error estimates of projection methods for Navier–Stokes equations: second-order schemes*, Mathematics of Computation, 65 (215) (1996), pp.1039–1065.
[52] J. Shen and J. Xu, *Convergence and error analysis for the scalar auxiliary variable (SAV) schemes to gradient flows*, SIAM Journal on Numerical Analysis, 56 (5) (2018), pp. 2895-2912
[53] J. Shen, J. Xu and J. Yang, *The scalar auxiliary variable (SAV) approach for gradient flows*, Journal of Computational Physics, 353 (2018), pp.407-416.
[54] L. Timmermans, P. Minev and F. Van De Vosse, *An approximate projection scheme for incompressible flow using spectral elements*, International Journal for Numerical Methods in Fluids, 22 (7) (1996), pp.673-688.
[55] R. Temam, *Sur l'approximation de la solution des équations de Navier-Stokes par la méthode des pas fractionnaires (II)*, Archive for Rational Mechanics and Analysis, 33 (1969), pp.377-385.